Asian Journal of Chemistry; Vol. 30, No. 11 (2018), 2450-2454
ASIAN JOURNAL OF CHEMISTRY
https://doi.org/10.14233/ajchem.2018.21443

Molecular Dynamics Simulation Study of Colloidal Suspensions under Confinement

P. UDAY KUMAR and R.N. BEHERA*

Department of Chemistry, Birla Institute of Technology & Science, Pilani-K.K. Birla Goa Campus, Zuarinagar-403 726, India

*Corresponding author: Fax: +91 832 2557031; Tel: +91 832 2580331; E-mail: rbehera@goa.bits-pilani.ac.in

Received: 14 May 2018; *Accepted*: 29 June 2018; *Published online*: 27 September 2018; AJC-19093

The density profiles and self-diffusion coefficients of model colloidal suspensions confined between two parallel walls have been studied using classical molecular dynamics simulation. The colloidal suspensions are modeled as asymmetric mixture of spherical particles interacting *via* Weeks-Chandler-Andersen (WCA) and Coulomb potential. Both the charged as well as neutral walls are considered. Systematic variations in density profiles as well as the self-diffusion coefficients are found with the size and charge of the colloid and with the kind of walls.

Keywords: Molecular dynamics simulation, Density profile, Self-diffusion coefficient, Colloid, Confinement.

INTRODUCTION

Colloidal suspensions are abundant in our day to day experience and used in numerous applications in chemical, mechanical, pharmaceutical, food industries, *etc*. [1-4]. Colloids have been found useful in composing "intelligent materials" as they can be both prepared and characterized in a controlled way [5], *e.g.* the effective interaction between the colloidal particles can be tailored by changing the system parameters [6]. Besides having considerable technological importance, colloidal suspensions are playing an increasingly important role as model systems to study, in real space, a variety of phenomena in condensed matter physics [7,8].

The colloidal suspensions under confinement can have interesting properties [9]. When the confining length (the distance between opposing boundaries) becomes comparable to the intrinsic length scale of the colloid particle, the confined suspension can behave quite differently from an identical suspension in the bulk [10-14]. Narrow confinement tends to lower the particle entropy and induces microscopic ordering of colloids into layers parallel to the confining walls [15]. This ordering is usually characterized by the density profile $\rho(z)$ across the confining walls. This density profile gives the distribution of particles across the walls and depends on the particle-particle and particle-wall interactions. The effects of confinement on structural and dynamics properties of colloids have given rise to many interesting phenomena [16-22]. Both simulation [23] and experimental [24] studies show the shift of the glass transition relative to bulk glass transition. The phenomena of drying [25] and freezing [26] transitions in confinement have created interest to study the behaviour of colloids in spatial two-dimension [27-29]. Also, the diffusion coefficient of the binary colloidal mixtures have been studied in confined geometries [30], slit shaped nanochannels [31,32], cylindrical pores [33], rectangular nanotubes [34,35] and within spherical cavity [36].

In this paper, we have employed the molecular dynamics simulations to study the molecular distribution and diffusion of model colloidal suspensions confined between two parallel walls. The walls are separated by a distance h along z-axis and are placed on the top and bottom of the simulation box (Fig. 1 shows schematic representation of the confinement). We have focused on the density profiles which are related to the interactions.

EXPERIMENTAL

We have used the primitive model and viewed the colloidal suspension as an asymmetric binary mixture consisting of negatively charged spherical colloid (type 0) and positively charged small ions (type 1) of diameter σ_i, (i = 0, 1) in a continuum solvent, interacting with the pair potential:

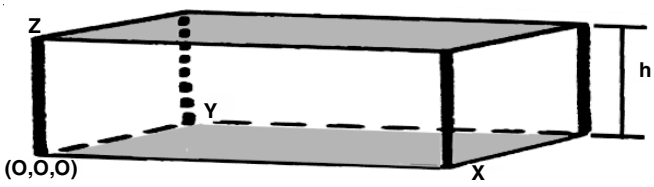

Fig. 1. Schematic representation of the simulation box and the positions of walls at the top and bottomof the simulation box

$$u_{ij}(r) = u_{ij}^{WCA} + u_{ij}^{C} \quad (1)$$

where the truncated and shifted Lennard-Jones potential (also known as Weeks-Chandler-Anderson potential) given by

$$u_{ij}^{WCA}(r) = \begin{cases} u_{ij}^{LJ}(r) - u_{ij}^{LJ}(r_c), & r < r_c \\ 0, & r > r_c \end{cases} \quad (2)$$

with, $u_{ij}^{LJ}(r) = 4\varepsilon_{ij}[(\sigma_{ij}/r)^{12} - (\sigma_{ij}/r)^{6}]$. The Coulomb potential (only for particles having charges) is given by $u_{ij}^{C}(r) = \beta L_B Z_i Z_j / r$. In the above expressions, the cut-off distance, $r_c = 2^{1/6}\sigma_{ij}$, $\sigma_{ij} = (\sigma_i + \sigma_j)/2$, $\varepsilon_{ij} = \sqrt{\varepsilon_i \varepsilon_j}$, σ_i and ε_i are Lennard Jones parameters, r is the inter particle distance, Z_i are charges, $L_B = \beta e^2/\varepsilon$ is the Bjerrum length, $\beta = 1/(k_b T)$ is the inverse temperature, k_b is the Boltzmann constant, T is the temperature, ε is the dielectric constant of the medium. The density profile of particle α is calculated by [37]:

$$\rho_\alpha(z) = \frac{\langle N_\alpha(z, z+\Delta z)\rangle}{A\Delta z} \quad (3)$$

where $\langle N_\alpha(z, z + \Delta z)\rangle$ is the average number of particles in a layer of thickness Δz around z and A is the area of the walls. In our case, $\Delta z = L_Z/20$. We have reported our results in terms of reduced density $\rho^* = \rho\sigma^3$. The diffusion coefficient of particle α is calculated from the slope of mean square displacement (MSD) at large times (along xy direction) according to Einstein relation [38]:

$$D_\alpha = \lim_{t\to\infty} \frac{\langle [r_\alpha(t) - r_\alpha(0)]^2 \rangle}{6t} \quad (4)$$

where, $r_\alpha(t)$ is the position of the particle in the xy plane at time t and $\langle ....\rangle$ denotes the ensemble averaging.

All the simulations were carried out in NVT ensemble. The Langevin thermostat [39] was used to maintain a constant temperature, which also provided the surrounding solvent conditions implicitly. Velocity Verlet scheme [40] was used for integrating the equation of motion using ESPResSO molecular dynamics simulation package [41]. Two confining parallel walls, one at the bottom and the other one at the top of the simulation box (normal of the wall pointing up and down along z-axis), are created using the inbuilt function "constraint wall" of the ESPResSO package. Partial periodic boundary conditions (along x and y directions) are used. The type of the wall is used like a particle type to define the interaction of the walls with the particles. MMM2D algorithm was used for confined systems [42]. Simulations were carried out for colloidal suspensions with total number of particles N (2100 to 5600) packed in an asymmetric box of dimension $L_X = L_Y = 1414$ nm, $L_Z = 500$ nm, under partial periodic boundary conditions (along x and y directions) with density in the range 2×10^{-7} atoms/nm^3 to 5.6×10^{-6} atoms/nm^3. The number of colloids, counter ions and the wall charges were adjusted to maintain the electroneutrality condition of the entire system. From the total simulation time of 20.4 ns, properties were calculated from the last 10.4 ns with the integration steps of at most 300 steps (1.8 ps). This MD program package we use has been successfully applied in the past [43] to calculate the equilibrium properties and diffusion coefficients for asymmetric electrolytes.

RESULTS AND DISCUSSION

We simulated the colloidal suspensions under the confinement of two parallel walls placed at the bottom and top of the simulation box (walls are parallel to xy plane). Both charged as well as neutral colloidal suspensions are considered. The diameters and charge used for the colloid (type 0 particle) are $\sigma_0 = 20$, 32, 40, 60 nm and $Z_0 = 0$ (neutral), -10e, -25e. The diameter and charge of counter ion (type 1 particle) are fixed at $\sigma_1 = 0.30$ nm and $Z_1 = 0$ (neutral) or 1e. We use three types of walls: (i) both neutral, (ii) both negatively charged (-1e) and (iii) one positively charged (1e) and one negatively charged (-1e). We report the variations of density distribution $\rho_i(z)$ and the self-diffusion coefficient (along the xy plane) D_i of the constituent particles (i = 0, 1) as a function of colloid diameter (σ_0) and colloid charge (Z_0) in the above chosen systems.

Density profile: In Fig. 2(a), we have compared the variations of colloid density profile ($\rho_0(z)$) for the systems with neutral colloid of different sizes confined between neutral walls. For the colloid with $\sigma_0 = 20$ nm, the density is more or less uniform except a small build up close to the walls (around 73 and 445 nm). As the colloid size increases (to 40 and 60 nm), there is a clear building up of density at various distances within the walls (z = ~ 50, 200, 400, 450 nm), indicating a layered distribution of colloid. The density is found to be at minimum at around layer of 250 to 300 nm (around the middle of the walls) and maximum close to the walls (z = 60 and 440 nm). Replacing the neutral walls with negatively charged walls, the density profile for the colloid (Fig. 2b) become less structured, the peak for $\sigma_0 = 20$ nm has moved away from the walls. The density distributions for the counter ions (Fig. 3) show layered distributions, shifting toward the upper wall with increase in colloid diameters.

The variation of colloid density profile with its charge confined between neutral walls (with $\sigma_0 = 32$ nm) is shown in Fig. 4a and for the charged walls is shown in Fig. 4b. We have taken colloid charge of -10e and -25e along with a neutral one (charge zero) for comparison. As clear from the plots, the neutral colloid density profile is more structured with build-up of density (roughly around 32, 300 and 450 nm). As the charge increases from zero to -10e (Fig. 4a), the colloids are pushed away from the walls (more from the bottom wall); two broad peaks (below z = 250 nm) merge to one and the profile becomes smooth. On further increase of charge to -25e (Fig. 4b), a similar build-up of density near walls appear. As the charge increases, the density is more or less symmetrical with average values at the middle of the walls and maxima around 1/4th from both the walls. The counter-ion density profile for the charged colloids between charged walls is displayed in

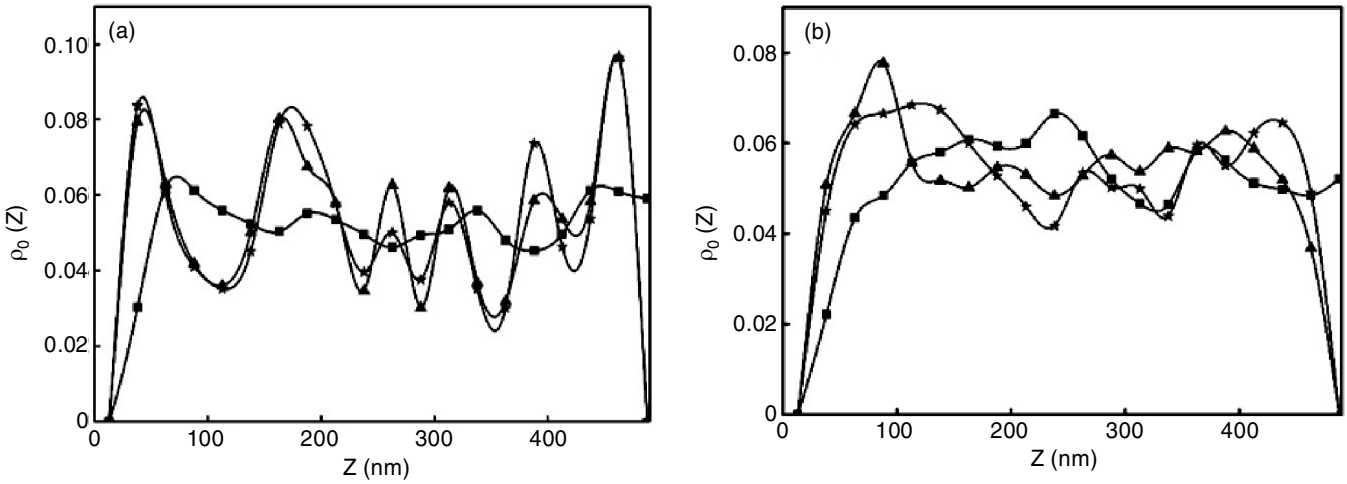

Fig. 2. Variation of colloid density profiles in neutral colloidal suspensions of different diameters in between two walls: (a) neutral walls, (b) negatively charged walls (symbols: square denotes σ_0 = 20 nm, triangle denotes σ_0 = 40 nm and star denotes σ_0 = 60 nm)

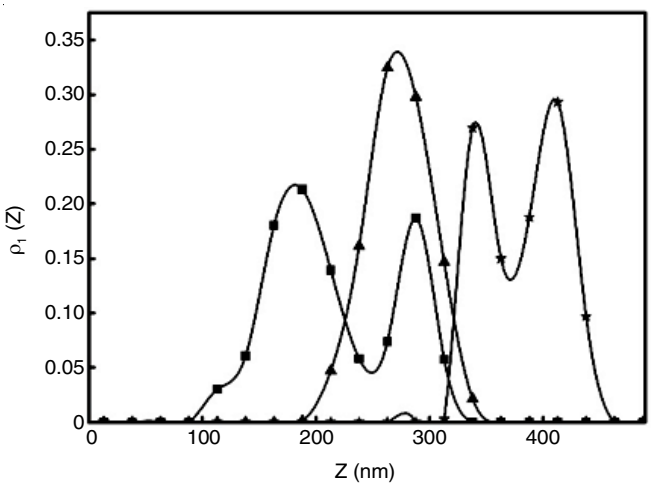

Fig. 3. Variation of small ion/particle density profiles in neutral colloidal suspensions of different diameters in between two negatively charged walls. Other parameters are same as in Fig. 2

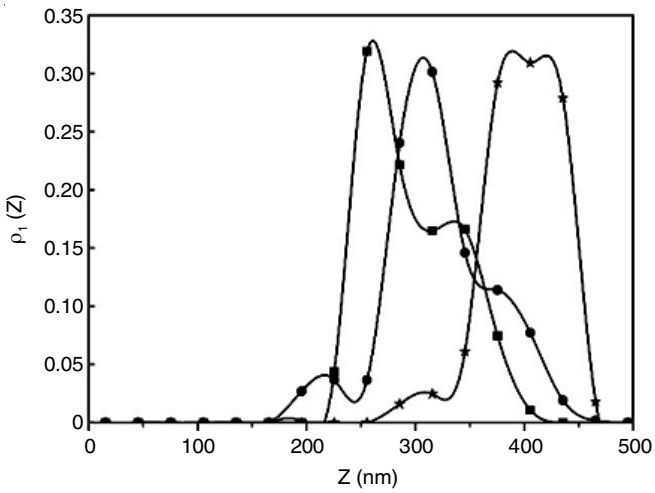

Fig. 5. Variation of counter ion density profiles with different colloidal charges for the colloidal suspensions of diameter σ_0 = 32 nm between two negatively charged walls. Other parameters are same as in Fig. 4

Fig. 5. The counter ion is distributed in layer roughly in the midway between the two walls for $Z_0 = 0$ case and shift towards the upper wall as the colloid charge increases.

In order to see the effects of different kinds of walls as described in the beginning of the section, on colloid profile, we carry out simulations for a colloidal suspensions with

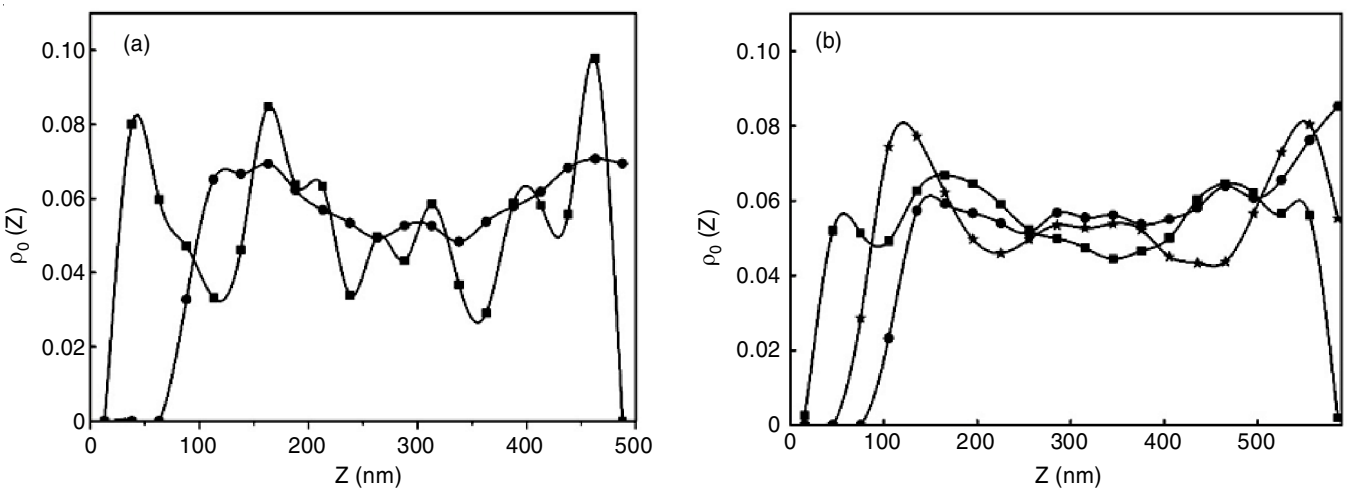

Fig. 4. Variation of colloid density profiles with different colloidal charges for the colloidal suspensions of diameter σ_0 = 32 nm: (a) between two neutral walls, (b) between two negatively charged walls (symbols: square indicates $Z_0 = 0$ (neutral), circle indicates Z_0 = -10e and star indicates Z_0 = -25e)

σ_0 = 20 nm and Z_0 = 25e. The result is shown in Fig. 6. For the case of neutral walls, the density profile increases from zero reaches a maxima and then fall to an average value as we go away from the wall. For the case of charged walls, we find a similar trend in density profile, but the values of maxima differ. For the case of both negatively charged walls, the magnitude of maxima close to bottom wall is less and that close to upper wall is more compared to the corresponding case for neutral walls; whereas for the case of (bottom positively and top negatively) charged walls, the peak height closer to positive wall increase (peak position more closer to wall) and that close to negative wall slightly decreases. Also, appearance of additional density distributions are found in the midway between the walls for oppositely charged walls.

Self-diffusion coefficient: Representative plots for the mean-square displacement (MSD) for type 0 (colloid) and type 1 (small ion) particle as a function of simulation time is displayed in Fig. 7. The MSD decreases in case of charged colloidal system/charged walls, as compared to the neutral colloidal system/neutral walls. The decrease in type 0 particle (colloid) is more compared to that for smaller ion (type 1 particle).

The self-diffusion coefficient of both the colloid and small ion/particle (D_0 and D_1) for various systems are presented in Fig. 8. The variation of D_i (i = 0, 1) as a function of colloid diameter for neutral colloid confined in charged walls is plotted in Fig. 8(a). As the colloid diameter increases, the value of D_0 systematically decreases while the value of D_1 increases and finally levels up. The variations in D_i (i = 0, 1) are much similar

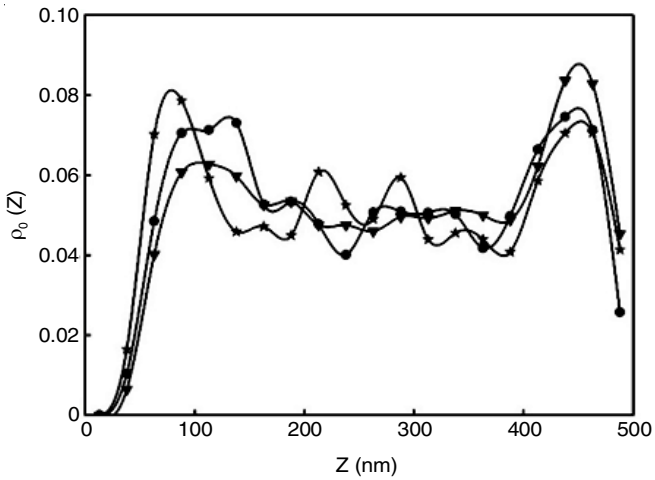

Fig. 6. Variation of colloid density profiles with different types of walls for the colloidal suspensions of diameter σ_0 = 20 nm and charge Z_0 = -25e. (symbols: circle indicates neutral wall on both sides, star indicates negatively charged wall on both sides (- -) and inverted triangle indicates oppositely charged wall on both sides (+ -))

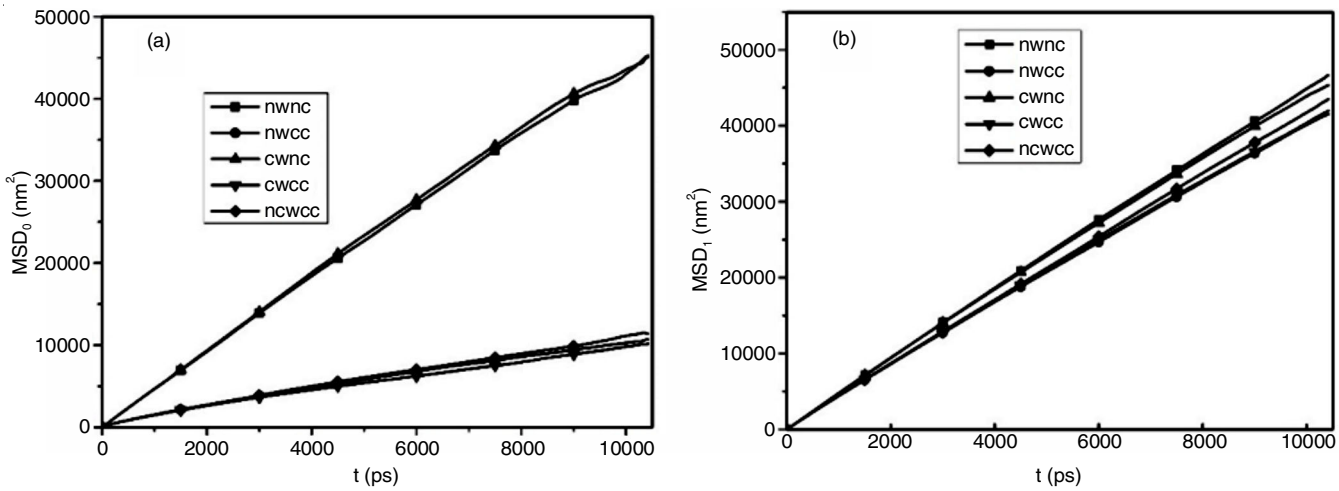

Fig. 7. Representative plotsfor variation of (a) colloid-colloid, (b) counterion-counterion, mean-square displacement (MSD) with simulation time for the colloidal suspension (σ_0 = 20 nm, Z_0 = -25e) with different confinement. (the first two lines from the top are for systems with neutral colloid in neutral and charged walls, next three lines are for systems with charged colloid with three kinds of wall described in Fig. 6)

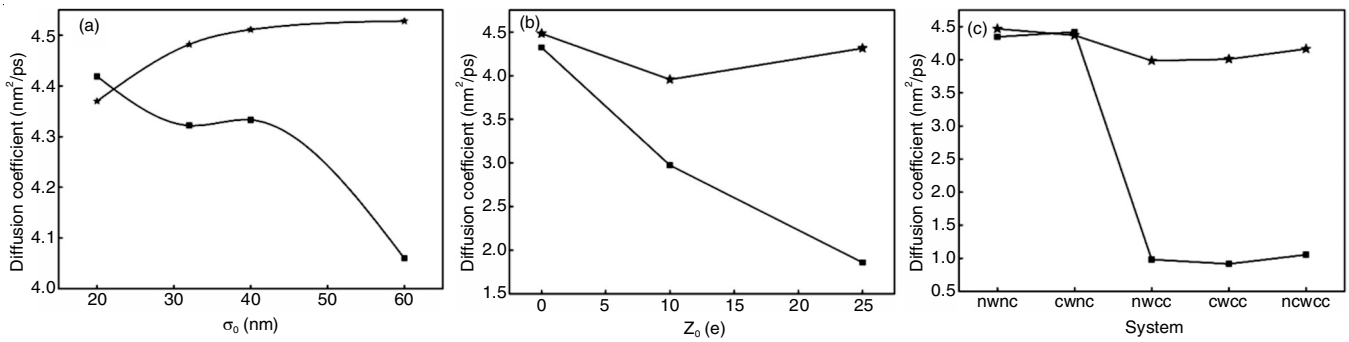

Fig. 8. Self-diffusion coefficient of colloid (square) and small ion/particle (star) for various colloidal suspensions under confinement: (a) variation with colloid size, (b) variation with colloid charge, (c) variation with different types of walls. The wall types are same as in Fig. 6

with increase in the charge of colloid (Fig. 8b) though the decrease of D_0 with Z_0 is more drastic. Finally, we have compared (Fig. 8c) the diffusion coefficients D_i for different types of colloidal suspensions in different types of walls studied. It is clear from the graph that the value of D_0 of neutral colloid is higher than those of charged colloid, irrespective of the types of wall. A similar trend in D_1 is observed, although the decrease in magnitude is very small. Self-diffusion coefficient of type 0 particle for charged colloidal particle with uncharged wall is less compared to the neutral colloidal particle of uncharged wall and the trend is same in charged colloid with charged wall when compared to neutral colloid with charged wall. The self-diffusion coefficient of type 1 particle for charged colloid system with charged and neutral wall is nearly same. However for neutral colloidal system with charged wall the self-diffusion coefficient is less compared to neutral wall.

Conclusion

We have carried out molecular dynamics simulation of both charged and uncharged colloidal suspensions between two parallel (charged and uncharged) walls. The variations in density profile functions and diffusion coefficients are studied as a function of colloid size, colloid charge and wall types. The density profiles functions for colloid become oscillatory indicating ordering/layering of particles. The oscillatory behaviour is found to be pronounced for colloid with neutral walls or one positive and one negative wall. A systematic variation in the density profile of small particle/ion is also observed. The self-diffusion coefficient of neutral colloid is found to be higher than that of charged one irrespective of the nature of walls.

ACKNOWLEDGEMENTS

The authors gratefully acknowledge the financial support from CSIR, India under Project No. 01(2513)/11/EMR-II. The use of DST-FIST supported computational facility of the Department as well as Central Computing Facility of Institute (Kosambi) during this work is also gratefully acknowledged.

CONFLICT OF INTEREST

The authors declare that there is no conflict of interests regarding the publication of this article.

REFERENCES

1. D.F. Evans and H. Wennerstrom, The Colloidal Domain: Where Physics, Chemistry, Biology and Technology Meet, Wiley-VCH, edn 2 (1999).
2. N. Geerts and E. Eiser, *Soft Matter*, **6**, 4647 (2010); https://doi.org/10.1039/c001603a.
3. E. Dickinson, *Annu. Rev. Food Sci. Technol.*, **6**, 211 (2015); https://doi.org/10.1146/annurev-food-022814-015651.
4. R. Jurgons, C. Seliger, A. Hilpert, L. Trahms, S. Odenbach and C. Alexiou, *J. Phys. Condens. Matter*, **18**, S2893 (2006); https://doi.org/10.1088/0953-8984/18/38/S24.
5. L. Belloni, *J. Phys. Condens. Matter*, **12**, R549 (2000); https://doi.org/10.1088/0953-8984/12/46/201.
6. C.N. Likos, *Phys. Rep.*, **348**, 267 (2001); https://doi.org/10.1016/S0370-1573(00)00141-1.
7. H. Lowen, *J. Phys. Condens. Matter*, **13**, R415 (2001); https://doi.org/10.1088/0953-8984/13/24/201.
8. W. Poon, *Science*, **304**, 830 (2004); https://doi.org/10.1126/science.1097964.
9. J. Klafter and J.M. Drake, Molecular Dynamics in Restricted Geometries, Wiley: New York (1989).
10. P. Pieranski, L. Strzelecki and B. Pansu, *Phys. Rev. Lett.*, **50**, 900 (1983); https://doi.org/10.1103/PhysRevLett.50.900.
11. D.H. Van Winkle and C.A. Murray, *Phys. Rev. A*, **34**, 562 (1986); https://doi.org/10.1103/PhysRevA.34.562.
12. J. Weiss, D.W. Oxtoby, D.G. Grier and C.A. Murray, *J. Chem. Phys.*, **103**, 1180 (1995); https://doi.org/10.1063/1.469828.
13. E. Chang and D. Hone, *Europhys. Lett.*, **5**, 635 (1988); https://doi.org/10.1209/0295-5075/5/7/011.
14. E. Allahyarov, I. D'Amico and H. Lowen, *Phys. Rev. E Stat. Phys. Plasmas Fluids Relat. Interdiscip. Topics*, **60**, 3199 (1999); https://doi.org/10.1103/PhysRevE.60.3199.
15. C. Stubenrauch and R.V. Klitzing, *J. Phys. Condens. Matter*, **15**, R1197 (2003); https://doi.org/10.1088/0953-8984/15/27/201.
16. W.A. Ducker, T.J. Senden and R.M. Pashley, *Nature*, **353**, 239 (1991); https://doi.org/10.1038/353239a0.
17. J.N. Israelachvili and R.M. Pashley, *Nature*, **306**, 249 (1983); https://doi.org/10.1038/306249a0.
18. S.H.L. Klapp, D. Qu and R. v. Klitzing, *J. Phys. Chem. B*, **111**, 1296 (2007); https://doi.org/10.1021/jp065982u.
19. Y. Zeng, S. Grandner, C.L.P. Oliveira, A.F. Thu¨nemann, O. Paris, J.S. Pedersen, S.H.L. Klapp and R. von Klitzing, *Soft Matter*, **7**, 10899 (2011); https://doi.org/10.1039/c1sm05971h.
20. H.H. von Gru¨nberg, L. Helden, P. Leiderer and C. Bechinger, *J. Chem. Phys.*, **114**, 10094 (2001); https://doi.org/10.1063/1.1371556.
21. B. Pouligny, D.J.W. Aastuen and N.A. Clark, *Phys. Rev. A*, **44**, 6616 (1991); https://doi.org/10.1103/PhysRevA.44.6616.
22. D.G. Grier and Y. Han, *J. Phys. Condens. Matter*, **16**, S4145 (2004); https://doi.org/10.1088/0953-8984/16/38/028.
23. T. Fehr and H. Lowen, *Phys. Rev. E Stat. Phys. Plasmas Fluids Relat. Interdiscip. Topics*, **52**, 4016 (1995); https://doi.org/10.1103/PhysRevE.52.4016.
24. C.R. Nugent, K.V. Edmond, H.N. Patel and E.R. Weeks, *Phys. Rev. Lett.*, **99**, 025702 (2007); https://doi.org/10.1103/PhysRevLett.99.025702.
25. S. Singh, J. Houston, F. van Swol and C.J. Brinker, *Nature*, **442**, 526 (2006); https://doi.org/10.1038/442526a.
26. O.A. Vasiley, S. Dietrich and S. Kondrat, *Soft Matter*, **14**, 586 (2017); https://doi.org/10.1039/C7SM01363A.
27. J. Bleibel, A. Dominguez and M. Oettel, *Phys. Rev. E*, **95**, 032604 (2017); https://doi.org/10.1103/PhysRevE.95.032604.
28. G. Wu, H. Cho, D.A. Wood, A.D. Dinsmore and S. Yang, *J. Am. Chem. Soc.*, **139**, 5095 (2017); https://doi.org/10.1021/jacs.6b12975.
29. H. Lowen, *J. Phys. Condens. Matter*, **21**, 474203 (2009); https://doi.org/10.1088/0953-8984/21/47/474203.
30. K. Nygard, *Phys. Chem. Chem. Phys.*, **19**, 23632 (2017); https://doi.org/10.1039/C7CP02497E.
31. R. Bhadauria and N.R. Aluru, *J. Chem. Phys.*, **145**, 074115 (2016); https://doi.org/10.1063/1.4961226.
32. U.M. Bettolo Marconi, P. Malgaretti and I. Pagonabarraga, *J. Chem. Phys.*, **143**, 184501 (2015); https://doi.org/10.1063/1.4934994.
33. S.T. Cui, *J. Chem. Phys.*, **123**, 054706 (2005); https://doi.org/10.1063/1.1989314.
34. R. Devi, S. Srivastava and K. Tankeshwar, *Phys. Chem. Liq.*, **52**, 636 (2014); https://doi.org/10.1080/00319104.2014.904860.
35. P.K. Yuet, *Langmuir*, **22**, 2979 (2006); https://doi.org/10.1021/la052736l.
36. C. Aponte-Rivera, Y. Su and R.N. Zia, *J. Fluid Mech.*, **836**, 413 (2018); https://doi.org/10.1017/jfm.2017.801.
37. J. Alejandre, M. Lozada-Cassou, E. González-Tovar and G.A. Chapela, *Chem. Phys. Lett.*, **175**, 111 (1990); https://doi.org/10.1016/0009-2614(90)85527-J.
38. A. Einstein, Investigation on the theory of Brownian Movement, Dover: New York (1926).
39. P.H. Hünenberger, *Adv. Polym. Sci.*, **173**, 105 (2005); https://doi.org/10.1007/b99427.
40. M.P. Allen and D.J. Tildesley, Computer Simulation of Liquids, Oxford University Press: New York (1991).
41. H.J. Limbach, A. Arnold, B.A. Mann and C. Holm, *Comput. Phys. Commun.*, **174**, 704 (2006); https://doi.org/10.1016/j.cpc.2005.10.005.
42. A. Arnold and C. Holm, *Comput. Phys. Commun.*, **148**, 327 (2002); https://doi.org/10.1016/S0010-4655(02)00586-6.
43. U.K. Padidela, T. Khanna and R.N. Behera, *Phys. Chem. Liq.*, **56**, 685 (2018); https://doi.org/10.1080/00319104.2017.1407932.